TRENDS IN SCIENCES 2026; 23(8): 12983
https://doi.org/10.48048/tis.2026.12983 RESEARCH ARTICLE

Catalytic Conversion of Pyrolysis Oil into Liquid Hydrocarbon Fuel via Deoxygenation Using Solid Pyrolysis Products of Buton Rock Asphalt

Vicario Baroroh[1], Didik Prasetyoko[1], Stella Jovita[1], Jasmin Nur Anggia[1], Brigyta Savariell Kurniawan[1], Anggoro Dias Ainur Rasyid[2], Hasliza Bahruji[3], Khawiyatur Rivah[1], Ingelia Yuan Fernanda[1], Trias Alzatory Ersyada[1], Anjas Abimanyu[1], Nurul Asikin Mijan[4] and Suprapto Suprapto[1,*]

[1]*Department of Chemistry, Faculty of Science and Data Analytics, Institut Teknologi Sepuluh Nopember, Surabaya 60111, Indonesia*
[2]*Departement of Civil Engineering, Faculty of Engineering, Universitas Negeri Surabaya, Surabaya 60232, Indonesia*
[3]*Centre for Advanced Material and Energy Sciences, Universiti Brunei Darussalam, Gadong BE1410, Brunei*
[4]*Departement of Chemistry, Faculty of Science and Technology, University Kebangsaan Malaysia, Bangi 43600, Malaysia*

([*]Corresponding author's e-mail: suprapto@chem.its.ac.id)

Received: 12 December 2025, Revised: 3 January 2026, Accepted: 10 January 2026, Published: 15 March 2026

Abstract

Asphalt Pyrolysis Oil (APO) obtained from Buton rock asphalt pyrolysis contains high oxygenate compounds, which cause the oil to be acidic and unstable; thus, it requires upgrading to improve its quality. Oxygenate compounds can be reduced by catalytic deoxygenation. This study utilized Buton rock asphalt solid residue (CRA), which is rich in $CaCO_3$, impregnated with Fe, Ni, and Zn metals as a deoxygenation catalyst (Fe/CRA, Ni/CRA, and Zn/CRA). GC-MS analysis revealed that the initial APO was predominantly composed of oxygenates and heavy fractions (C_{18} and above) (45.91%). After deoxygenation using Ni/CRA, the C_{11}-C_{18} fraction increased to 77.40% and the fraction greater than C_{18} decreased to 16.32%. The Ni/CRA catalyst also showed the best performance with the highest liquid yield (69.11%) and the lowest coke (1.42%). These results indicate that Fe/CRA, Ni/CRA, and Zn/CRA have the potential to improve the quality of APO liquid fuel.

Keywords: Asphalt pyrolysis oil, Liquid fuel upgrading, Buton rock asphalt, Catalytic deoxygenation, Metal impregnation.

Introduction

The high dependence on fossil fuels has significant consequences, particularly for the availability and stability of the energy supply. Fluctuations in global oil prices and limited conventional oil reserves pose risks to future energy security. Therefore, efforts are needed to find and utilize alternative oil sources that are abundant, competitive, and capable of ensuring a sustainable energy supply in the long term [1,2]. Buton rock asphalt (RA) is one of the abundant natural bitumen sources in Indonesia and holds great potential as an alternative raw energy material [1]. The high abundance of aromatic compounds, namely asphaltenes and maltenes in RA, has the potential to be converted into liquid fuels through selective thermal cracking [3]. However, fuel oil obtained from the pyrolysis of asphaltene-rich raw materials has low thermal stability, a low calorific value, a high-water content, and a high oxygen content [4,5]. The presence of these oxygenate compounds reduces oil quality because it increases acidity, chemical reactivity, and instability during storage [5]. Therefore, the oil from the pyrolysis of Buton asphalt (APO) requires upgrading through additional treatments. Oil upgrading treatment,

which includes distillation, solvent extraction, emulsification, catalytic esterification, deoxygenation, and catalytic cracking, is the most common technique used to improve oil quality [2]. The removal of oxygen from oil can be achieved through catalytic cracking at atmospheric pressure. However, this process has not been effectively used on a larger scale due to high coke formation and catalyst deactivation [2,6,7]. Catalytic deoxygenation can convert oxygenated compounds in oil into hydrocarbons and remove oxygen in the form of H_2O, CO, and CO_2 [2].

Various conventional base catalysts, such as CaO, commercial $CaCO_3$, dolomite, biochar, marble waste, and other mineral-based materials, have been widely reported for catalytic deoxygenation processes [2,8-10]. However, these approaches generally still use separately synthesized catalyst supports derived from new raw material sources. In the process of pyrolysis of Buton rock asphalt (RA), besides producing asphalt pyrolysis oil (APO), a solid residue is also formed in the form of charcoal residue asphalt (CRA), which is naturally rich in calcite as its main component [11]. $CaCO_3$ is known to have basic properties, high thermal stability, and potential as a catalyst support that can interact with oxygenate groups during the catalytic reaction process. The $CaCO_3$ content in CRA has the potential to be applied as a base catalyst that can increase conversion and reduce oxygen content in oil by decarboxylation and decarbonylation reactions [8,9]. Asphalt residue (CRA) catalysts offer advantages in terms of material availability, sustainability, and low production costs. However, pyrolysis-derived asphalt residue (CRA) generally has a low surface area, limited porosity, and contains some impurities that can reduce its effectiveness as a catalyst if not further treated [12]. To overcome these limitations, modification of the structure and composition of asphalt residue (CRA) was required. Hydrothermal treatment is a process of treating solid materials in an aqueous environment in a closed reactor (autoclave) with high pressure at medium temperature. Hydrothermal treatment has been demonstrated as an effective strategy to increase surface area and remove impurities, thereby improving catalytic activity [13]. Besides that, to increase the catalytic deoxygenation performance, doping of transition metals such as Ni, Fe, Zn into support materials has been systematically tried, which can highly promote the oil upgrading process [10,14,15].

Metal-based catalysts have a significant influence on the catalytic pyrolysis of fuel production [14]. Ni-dolomite catalysts exhibit outstanding catalytic activity and resistance to coking [16]. Incorporating calcium-based materials with nickel-based catalysts significantly enhances biomass pyrolysis, CO_2 removal, liquid macromolecule conversion, and gas composition adjustment [14]. The presence of Ni as promoters enhances hydrogenation reactions to remove oxygenate compounds and limit coke formation [17-20]. Maneechakr *et al.* [10] report that the loaded Fe in the zeolite tends to promote non-hydrogenative deoxygenation pathways through decarboxylation and decarbonylation reactions, which remove oxygen in the form of CO_2 and CO [10,21]. In addition, adding Zn to the ZSM-5 zeolite introduces Lewis acid sites that promote mild cracking and selective deoxygenation without accelerating excessive aromatization [15,22].

In this study, CRA was impregnated with Fe, Ni and Zn to increase catalytically active sites. This impregnation accelerates chemical reactions and increases product selectivity [23]. The CRA that had been combined with metal was calcined at 800 °C for 1 h to trigger phase transformation, improve the pore structure, and remove remaining volatile compounds [24]. The metal-impregnated CRA was then used as a catalyst in the deoxygenation process of asphalt pyrolysis oil (APO), a process known to increase the calorific value, thermal stability, and viscosity [25]. The use of metal-loaded CRA allows the integration of a circular economy concept, where pyrolysis solid waste is reused as a functional catalyst for upgrading its own liquid product [8,11]. To ensure the successful modification and effectiveness of the resulting catalyst, characterization of the physical and chemical properties of the catalyst and the resulting liquid product is necessary. X-ray diffraction (XRD) analysis was carried out to determine the material structure and transition metal phases dispersed on the surface of CRA. Fourier Transform Infrared (FTIR) was used to identify functional groups that play an important role in catalytic activity. To observe the surface morphology and distribution of metal elements, Field Emission-Scanning Electron Microscopy and Energy Dispersive X-Ray (FESEM-EDX) were used. Furthermore, to determine

textural parameters such as specific surface area, pore volume, and pore size distribution that affect the effectiveness of the reaction, Brunauer-Emmett-Teller (BET) and N_2 adsorption-desorption isothermal analysis were performed. In addition, to assess the quality of the liquid product from pyrolysis, Gas chromatography-mass spectrometry (GC-MS) analysis was carried out to determine the composition of hydrocarbon compounds in the resulting oil. With this characterization, it is hoped that a comprehensive representation can be obtained regarding the potential use of modified CRA from Buton rock asphalt pyrolysis as a heterogeneous catalyst in the development of high-quality liquid fuels.

Materials and methods

Materials

The materials used in this study included Buton rock asphalt pyrolysis oil (APO), Buton rock asphalt solid pyrolysis residue (CRA), nitrogen gas, distilled water, $Ni(NO_3)_2.6H_2O$ (Merck), $Fe(NO_3)_3{\cdot}9H_2O$ (Merck), $Zn(CH_3COO)_2.2H_2O$ (Merck), and hexane (Merck).

Catalyst synthesis

The catalyst synthesis is illustrated in **Figure 1**. Asphalt residue (CRA) of 5 g was ground and sieved using a 200-mesh sieve with a diameter of 0.075 mm. The metal catalysts, $Ni(NO_3)_2.6H_2O$, $Fe(NO_3)_3{\cdot}6H_2O$ (Merck), and $Zn(NO_3)_2.6H_2O$, were dissolved in 100 mL of distilled water and loaded onto the asphalt residue sample (CRA). The mixture was stirred for 1 h. The mixture obtained was hydrothermally autoclaved at 160 °C for 6 h. After that, the mixture was heated and stirred at 80 °C to remove the solvent. The slurry obtained was dried in an oven at 135 °C overnight. The solid obtained was then calcined at 800 °C for 1 h.

Characterization of the catalyst

The XRD analysis was conducted using an X-ray Diffraction (XRD) PHILIPS-binary XPert with MPD diffractometer with Cu Kα radiation operated at 30 mA and 40 kV and scanned from 10° to 60° to identify its chemical structure. The morphology and the surface analysis of Buton rock asphalt and the pyrolysis solid product obtained were analyzed using a scanning electron microscope (SEM), Hitachi Scanning Electron Microscope Flex SEM 1000, combined with the energy dispersive X-ray spectroscopy (EDX). N_2 Adsorption-Desorption was carried out to determine the specific surface area of the catalysts.

Catalytic deoxygenation of asphalt pyrolysis oil (APO)

The catalytic reaction was performed in a 100 mL 3-necked flask equipped with a distillation setup including a heating mantle and stirrer. A total of 3 g of catalyst was added to 10 g of asphalt pyrolysis oil (APO), which was pre-filtered using Whatman filter paper. The mixture was stirred and heated to 350 °C for 2 h under a constant N_2 flow at 20 mL/min. The liquid product was collected in a vessel that cooled to 18 °C to facilitate condensation. The obtained liquid products were collected from the outlet and analyzed using Gas Chromatography-Mass Spectrometry.

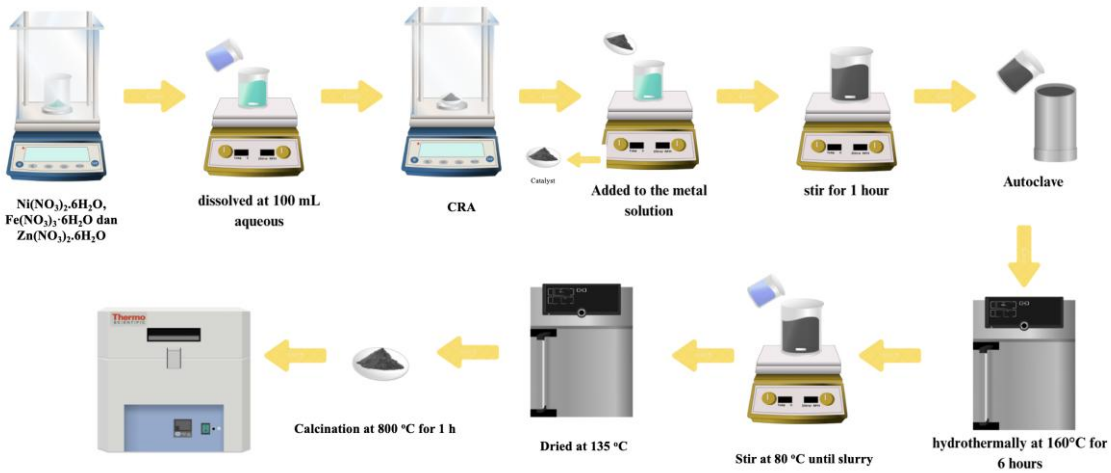

Figure 1 The scheme of catalyst synthesis.

Results and discussion

Characterization of the catalyst

Figure 2 shows the XRD analysis of CRA, Fe/CRA, Ni/CRA, and Zn/CRA catalysts. The diffraction pattern of the CRA indicated that its main composition is calcite ($CaCO_3$) as evidenced by the peaks at 2θ = 23.2°, 29.5°, 36.1°, 39.5°, 43.3°, 47.6°, and 48.6° (JCPDS 01-081-2027). After impregnation, the intensity of $CaCO_3$ in Fe/CRA and Ni/CRA decreased, followed by the appearance of strong diffraction peaks of $Ca(OH)_2$ at 2θ =17.88°, 28.57°, 34.1°, 47.04°, 50.78° and 54.33° (ICSD 01-084-1265) [26]. Thermodynamically, after calcination at 800 ºC during the impregnation process, CaCO3 decomposes into CaO. However, CaO was hygroscopic, so it reacts with water vapor through a hydration process when in contact with air after pyrolysis [10,15,27]. At the deoxygenation reaction temperature (350 °C), $Ca(OH)_2$ is still relatively stable and functions as a surface base site that supports the decarboxylation and decarbonylation reactions of oxygenate compounds [8,9]. The Fe/CRA sample showed peaks at 33.0°, 35.14°, 49.98° and 54.96°, which correspond to the Fe_2O_3 according to (JCPDS no. 33-0664) [28,29]. The Ni/CRA sample shows new sharp peaks at 2θ: 44.21° and 52.13°, identical to that of the crystallographic planes of pure Ni according to (JCPDS 001-1258) [30].

In contrast to the Fe/CRA and Ni/CRA catalysts, the $CaCO_3$ peak in the Zn/CRA catalyst still appears, with several weak $Ca(OH)_2$ peaks. This is due to the acidity and reactivity of metal ions formed during the hydrothermal stage. Fe^{3+} and Ni^{2+} ions are more acidic than Zn^{2+}, so they can accelerate the dissolution process of $CaCO_3$ through carbonic acid reactions during hydrothermal treatment, so that it can easily form $Ca(OH)_2$ [31]. Meanwhile, Zn^{2+} is an ion with weaker acidic properties. ZnO does not interact significantly with $CaCO_3$, even tends to stabilize it thermally, so that the $CaCO_3$ phase remains dominant in the Zn/CRA sample [32]. In addition, in the Zn/CRA sample, new peaks appear at 31.80°, 36.2° and 57.08°, which are typical of ZnO according to JCPDS 36-1451 [33]. Based on the XRD diffractogram, the CRA has a dominant calcite phase. However, after the impregnation and calcination processes, the structure was changed by the formation of active metal compounds (Fe, Ni, and Zn) and their oxides.

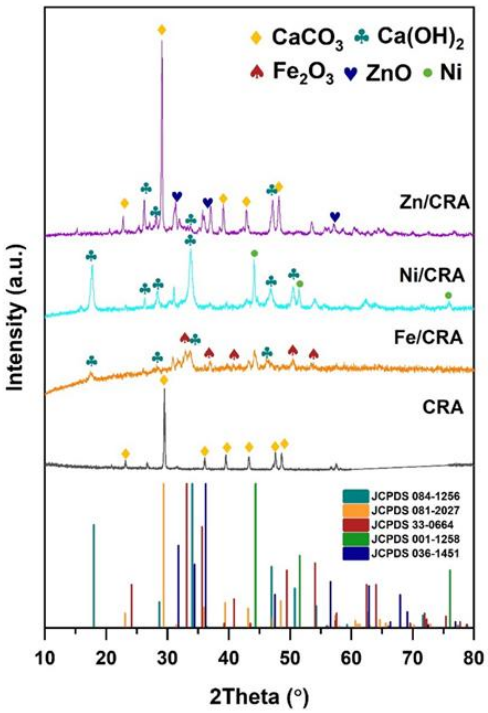

Figure 2 XRD pattern of CRA, Fe/CRA, Ni/CRA, and Zn/CRA.

The catalysts were characterized using FTIR spectroscopy to identify functional groups and verify the bonding interactions between the CRA and metal species. As shown in **Figure 3**, the absorption bands appearing at 3,500 - 3,641 cm^{-1} in all samples correspond to the O-H stretching vibrations, indicating the presence of surface hydroxyl groups [34]. In the CRA, a dominant band at 1,440 cm^{-1} is attributed to the asymmetric stretching of carbonate ions (CO_3^{2-}) from $CaCO_3$, while the bands at 889 and 711 cm^{-1} arise from the bending modes of CO_3^{2-}, further confirming the presence of calcium carbonate as the primary mineral phase [11]. The Fe/CRA catalyst, a distinct band appears at 518 cm^{-1}, corresponding to Fe-O stretching, indicating the formation of iron oxide species on the CRA surface. The presence of this band is consistent with Fe_3O_4 vibrational signatures typically reported in the 550 - 600 cm^{-1} region for mixed-valence iron oxides [35]. For the Ni/CRA sample, a characteristic band emerges at 545 cm^{-1}, assigned to the Ni-O vibrational mode, confirming the formation of NiO species dispersed on the CRA surface [36,37]. The Zn/CRA catalyst exhibits a strong band at 470 cm^{-1}, which is attributed to Zn-O stretching [38]. The FTIR spectra indicate that the characteristic carbonate bands are retained across all metal-modified catalysts, demonstrating that the $CaCO_3$ framework within the CRA support remains structurally intact following metal impregnation. This stability suggests that the incorporation of Fe, Ni and Zn does not disrupt the fundamental carbonate matrix. In contrast, the emergence of distinct M-O vibrational bands in the Fe/CRA, Ni/CRA, and Zn/CRA samples confirms the successful formation of metal oxide species on the CRA surface. The appearance of these metal–oxygen absorptions provides strong evidence of effective interaction between the deposited metals and the support, validating that the impregnation process leads to a well-integrated metal oxide phase.

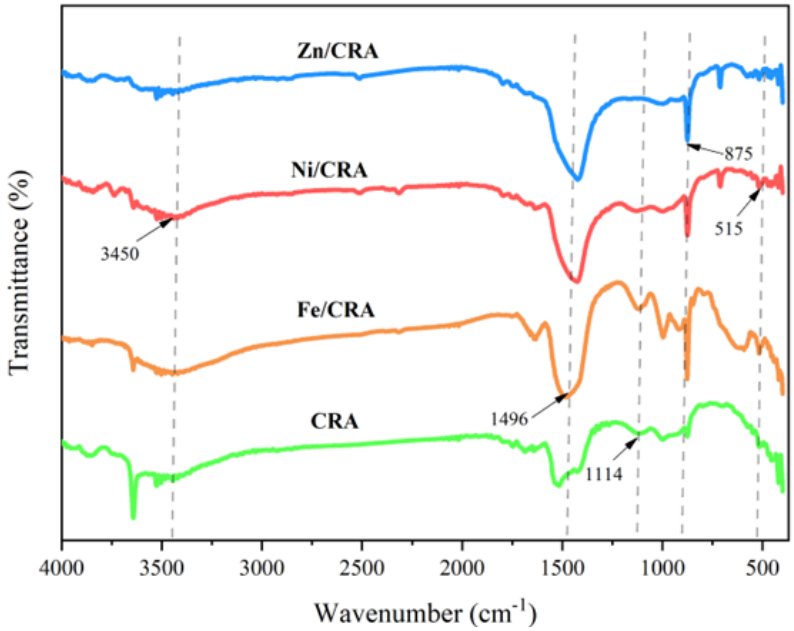

Figure 3 FTIR spectra of (CRA, Fe/CRA, Ni/CRA, and Zn/CRA).

The morphology and compositional characterization of CRA and Ni/CRA catalysts were performed using FESEM-EDX, as shown in **Figure 4** and **Table 1**. FESEM analysis of CRA shows an irregular, porous surface morphology, composed of carbon-mineral agglomerates with a rough texture, which is a common characteristic of calcium-based char resulting from the pyrolysis of bituminous materials. The element distribution in EDX mapping shows a dominance of Ca, C and O, which confirms that the CRA structure mainly consists of a $CaCO_3$ matrix, while the presence of Si, Al, Mg, and S reflects the inherent minerals of Buton rock asphalt [39]. After impregnation with Ni, the Ni/CRA surface exhibited a more compact

morphology with finer agglomerations, indicating that Ni partially covered the CRA. EDX spectra and mapping confirmed the presence of uniformly dispersed Ni on the surface, without forming large agglomerations, which is an important characteristic for Ni-based catalysts to enhance activity and surface accessibility.

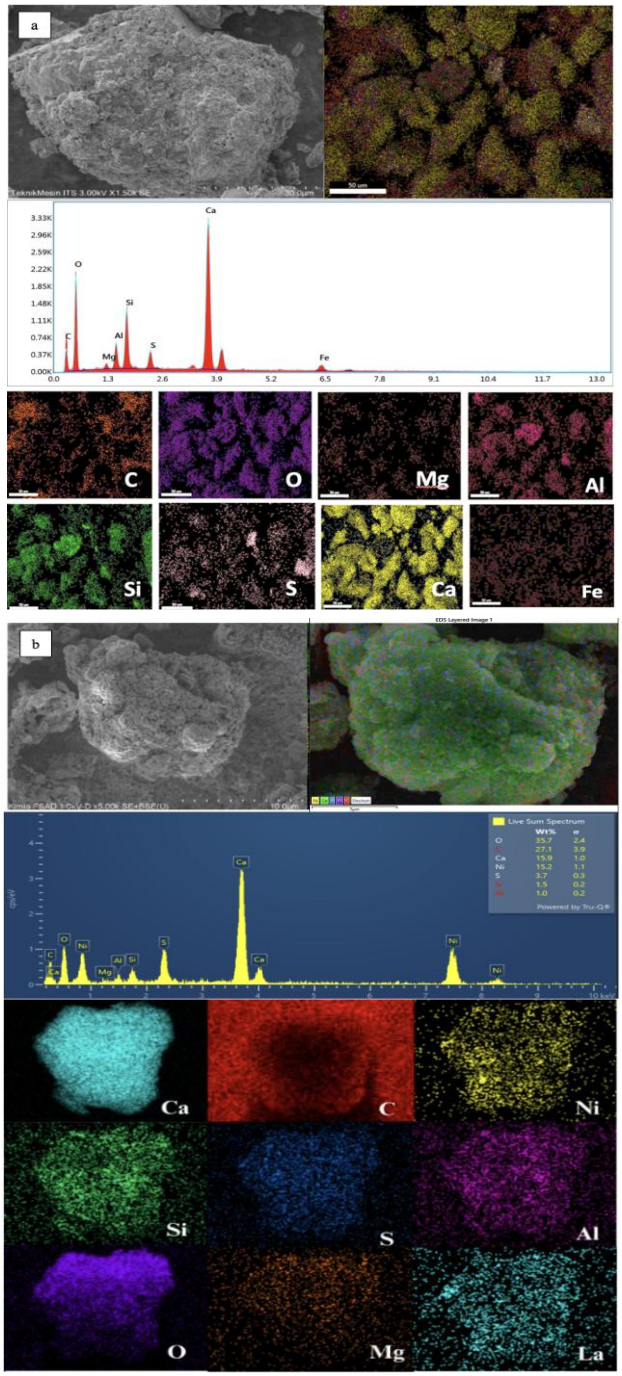

Figure 4 SEM-EDX analysis of a) CRA and b) Ni/CRA.

The elemental composition of the sample surface obtained through EDX analysis is shown in **Table 1**. Based on these data, before impregnation, the CRA sample did not contain nickel (Ni). However, after impregnation, Ni was detected in the Ni/CRA sample at a concentration of 15.2%. This indicates that metal impregnation using the wet method successfully distributed Ni to the CRA surface [40]. The calcium

(Ca) element, which initially dominated the CRA surface with a value of around 31.7%, decreased drastically to 15.9% in Ni/CRA. This decrease indicates that most of the areas that previously contained Ca were likely covered by Ni metal particles. In addition, other elements such as silicon (Si), aluminum (Al), and magnesium (Mg) also showed a decrease, which further strengthens the suspicion that the surface composition has changed due to the impregnation treatment.

Table 1 Elements of CRA and Ni/CRA.

Element	Catalyst	
	CRA (Wt%)	**Ni/CRA (Wt%)**
O	47.8	35.7
C	4.1	27.1
Ca	31.7	15.9
Ni	-	15.2
S	2.3	3.7
Si	6.6	1.5
Al	3.4	1
Mg	0.9	-
Fe	3.1	-

Textural characterization using the N_2 adsorption-desorption method on CRA, Fe/CRA, Ni/CRA, and Zn/CRA samples (**Figure 5** and **Table 2**) showed that modification with metal catalysts significantly affected the surface area, volume, and pore distribution. All samples exhibited type IV adsorption isotherms with hysteresis at P/P_o 0.4 - 1.0, which is typical of mesoporous. CRA before impregnation had the largest surface area (S_{BET} = 15.03 m^2/g) and the highest pore volume (V_{tot} = 0.0911 cc/g). After the metal impregnation process, the textural properties of the catalyst experienced significant changes in surface area and pore volume. especially in the Fe/CRA (S_{BET} = 4.52 m^2/g) and Zn/CRA (S_{BET} = 4.12 m^2/g) samples. This was caused by the clogging of pores in the CRA due to the presence of metal covering the CRA pores. The Ni/CRA catalyst showed better textural properties than Fe/CRA (S_{BET} = 4.52 m^2/g) and Zn/CRA (S_{BET} = 4.12 m^2/g). The specific surface area is 9.45 m^2/g with a pore volume of 0.0329 cm^3/g and an average pore size of 20.25 nm. This indicates that Ni does not completely block the pore structure of CRA [41]. A significant increase in the micropore area (5.71 m^2/g) is also seen, indicating that Ni can expand the internal structure of CRA, resulting in a combination of micro and mesoporous structures. The relatively wide pore distribution and peak in the range of 30 nm in **Figure 5(b)** indicate that Ni/RA has an open pore structure that strongly supports the diffusion process of reactant molecules.

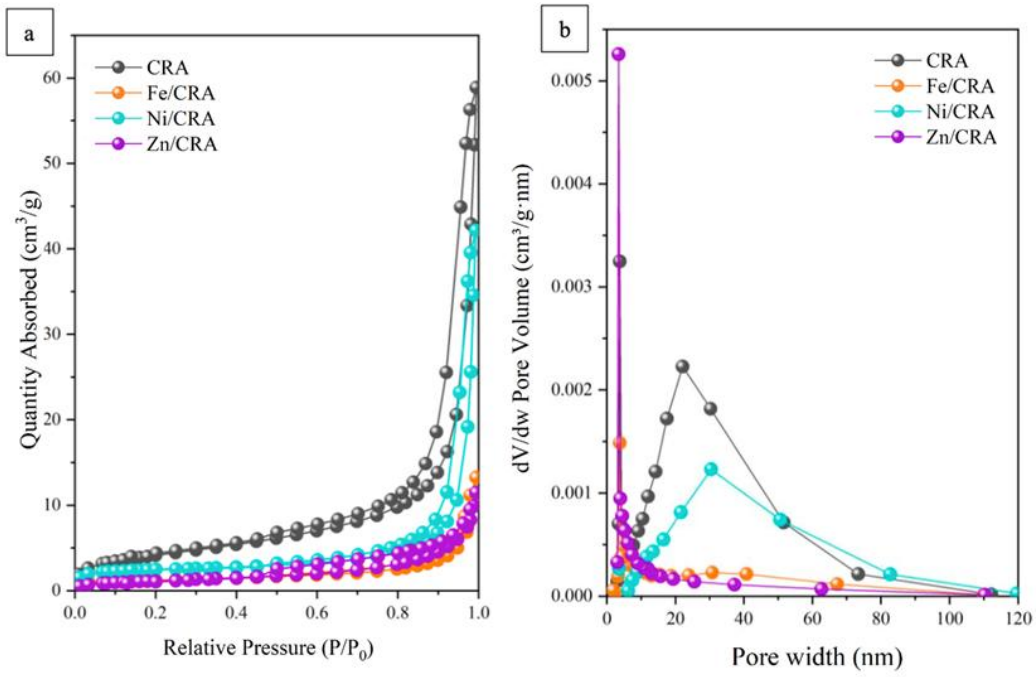

Figure 5 (a) N_2 adsorption-desorption isotherm and (b) Pore distribution of the catalyst.

Table 2 Pore distribution of CRA, Fe/CRA, Ni/CRA, and Zn/CRA catalysts.

Catalyst	Surface area (m^2/g)				Pore volume (cc/g)			Average pore width (nm)
	S_{BET}	S_{meso}	S_{ext}	S_{micro}	V_{meso}	V_{micro}	V_{tot}	
CRA	15.03	15.93	15.01	0.02	0.0910	0.0001	0.0911	22.8
Fe/CRA	4.52	4.02	2.51	2.01	0.0203	0.0008	0.0211	20.2
Ni/CRA	9.45	8.27	3.74	5.71	0.0647	0.0022	0.0329	30.4
Zn/CRA	4.12	6.53	4.23	-	0.0178	0.0001	0.0179	3.4

Deoxygenation of the liquid product using the catalyst

Figures 6(a) - 6(d) show the visual changes in the oil before and after the deoxygenation process. The initial asphalt pyrolysis oil (APO) has a darker color, indicating a high content of high-molecular-weight hydrocarbons, resins, light asphaltenes, and heavy oxygenate compounds, which are common in asphalt pyrolysis oil. **Figure 6(b)** shows the color change of the oil that was deoxygenated using the Fe/CRA catalyst, which becomes bright yellow and clear, indicating a decrease in oxygenate content and degradation of the complex aromatic structure. The oil deoxygenated with the Ni/CRA catalyst (**Figure 6(c)**) appears as the clearest and has the highest yield, indicating the effectiveness of the Ni/CRA catalyst. While the presence of Ni can break C-O bonds through hydrogenation reactions [14,20]. The oil deoxygenated with the Zn/CRA catalyst (**Figure 6(d)**) showed a pale-yellow color, slightly darker than Ni/CRA. ZnO acts as an effective Lewis acid catalyst for mild cracking and decarboxylation [22]. Overall, the oil color changes indicate that catalysts (Fe/CRA, Ni/CRA, Zn/CRA) can improve oil quality through the reduction of oxygenate compounds. However, Ni/CRA provides the better deoxygenation performance, indicated by the brightest oil product color and its clarity.

Figure 6 (a) APO, (b) Fe/CRA, (c) Ni/CRA, and (d) Zn/CRA catalyst deoxygenation products.

Figure 7 shows the distribution of liquid, gas, and coke fractions from the asphalt pyrolysis oil (APO) deoxygenated using Fe/CRA, Ni/CRA, and Zn/CRA catalysts. The use of the Fe/CRA catalyst resulted in lower liquid fractions (54.35%) and coke (4.66%). However, the gas fraction (10.84%) was higher, it is because Fe promotes the decarboxylation and dehydrogenation pathways, which produce CO/CO_2 and other gases in high quantities [21]. Besides that, Fe-CRA produces high cokes due to its high acidity. The catalyst with high acidity causes polymerization and polycondensation, where char is formed by the repolymerization reaction [10]. In contrast, the Ni/CRA catalyst produced the highest liquid fraction (69.11%) with the lowest coke (1.42%) compared to other catalysts. This reflects Ni's ability to carry out the hydrogenation and hydrogenolysis mechanisms, which not only enhance the conversion of oxygenate compounds to hydrocarbons but also limit coke formation via the carbon radical hydrogenation pathway [41]. The Zn/CRA catalyst produces a liquid yield of around 66.02% and a relatively low coke yield (4.06%). The Lewis acid nature of ZnO allows hydrocarbon cracking without accelerating aromatization, thus limiting coke formation [15]. Based on the results obtained, Ni/CRA is the most effective catalyst in maximizing the liquid fraction and minimizing coke, followed by Zn/CRA > Fe/CRA.

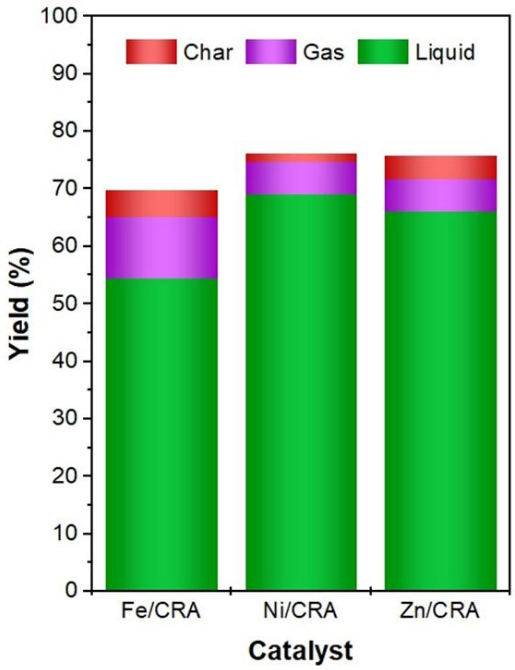

Figure 7 Conversion and yield of deoxygenation APO with catalyst Fe/CRA, Ni/CRA, Zn/CRA.

Characterization of liquid product (oil)

Gas chromatography-mass spectrometry (GC-MS) analysis of the initial asphalt pyrolysis oil (APO) and the catalytic deoxygenation product was carried out after dilution with n-hexane, as seen in **Figure 8**. The resulting chemical composition is divided into several types of compounds, including hydrocarbons, alcohols, ketones, phenols, aldehydes, esters, and carboxylic acids. The initial APO compound has a high oxygenate content (15.39%), making it acidic and unstable [18]. After deoxygenation using a metal/CRA catalyst, the total hydrocarbon yields significantly increased, while the oxygenated compounds decreased. This indicates that the catalysts were effective for the oil upgrading process [10]. Based on these results, Ni/CRA proved to be the best catalyst for improving oil quality because it achieved a total hydrocarbon yield of up to 65.03% and a decrease in oxygenated compounds to 3.97%. Meanwhile, the lowest quality of the upgraded oil was found in Fe/CRA. In Fe/CRA, the hydrocarbon fraction obtained was 49.08% with an oxygenate compound content of 4.915%. Zn/CRA produced a significant increase in hydrocarbons (63.16%), but slightly lower than Ni/CRA. The performance of Ni/CRA is influenced by the presence of acid sites, which make strong interactions with hydrocarbon compounds [10]. In addition, Ni induces hydrogenation and hydrogenolysis of oxygenate compounds (acids, ketones, esters), so it is effective in reducing oxygen content [19].

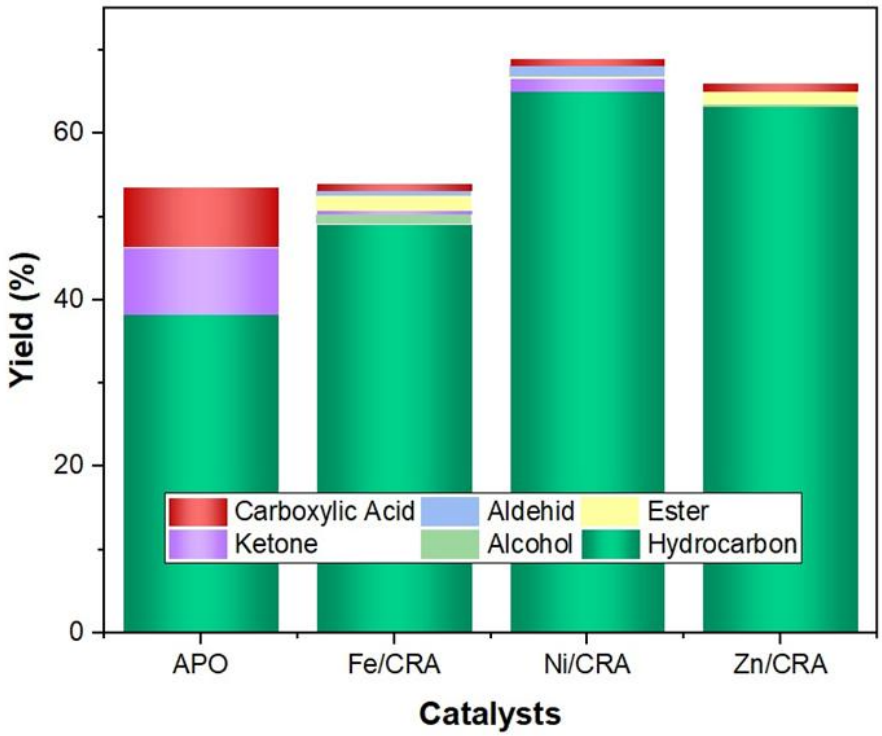

Figure 8 The distribution of APO deoxygenation product catalyzed using Fe/CRA, Ni/CRA, and Zn/CRA.

The degree of DO was further calculated using a semi-quantitative O/C ratio derived from GC-MS product distribution. The O/C ratio was estimated by considering the relative contribution of oxygenate compounds, including alcohols, ketones, aldehydes, esters, and carboxylic acids, based on their characteristic oxygen atom numbers. Based on **Table 3**, the initial asphalt pyrolysis oil (APO) exhibited a relatively high O/C ratio of 0.226, which is responsible for high acidity and poor stability. After catalytic DO, a substantial decrease in the O/C ratio was observed for all metal-loaded CRA catalysts, indicating effective oxygen removal. Among them, the Ni/CRA catalyst showed the lowest O/C ratio of 0.049, corresponding to an approximately 78% reduction compared to APO. This significant decrease confirms the efficient elimination of oxygen functionalities via hydrogenation, decarbonylation, and decarboxylation pathways. The

reduction in O/C ratio is consistent with the increased hydrocarbon fraction and the visual transformation toward a lighter and clearer oil, thereby providing quantitative evidence for the improved quality of the upgraded oil.

Table 3 Semi-quantitative O/C ratio from GC-MS of asphalt pyrolysis oil before and after catalytic deoxygenation.

Catalyst	O/C ratio
APO	0.226
Fe/CRA	0.079
Ni/CRA	0.049
Zn/CRA	0.054

Figure 9 shows the distribution of hydrocarbons based on their carbon number (C_8-C_{32}) for initial pyrolysis oil (APO) and deoxygenated product using Fe/CRA, Ni/CRA, and Zn/CRA catalysts. The APO hydrocarbon is dominated by long-chain compounds (C_{20}-C_{32}), which represent heavy fractions and complex oxygenates [42]. The Fe/CRA, Ni/CRA, and Zn/CRA catalysts' deoxygenation process has a significant effect on the distribution of the resulting hydrocarbons. All these catalysts convert the oil composition to a higher C_{11}-C_{18} fraction. However, the Fe/CRA catalyst still has a significant amount of C_{20}-C_{22} hydrocarbons, indicating that this catalyst was less effective in eliminating all heavy fractions. This is due to the nature of Fe, which tends to undergo decarboxylation reactions rather than cracking [21]. The hydrocarbon obtained using the Ni/CRA catalyst showed the highest C_{12}-C_{18} fraction. Meanwhile, the peak intensity in the C_{19}-C_{22} fraction decreased drastically, and the $>C_{22}$ fraction almost disappeared. This indicates that Ni/CRA undergo higher cracking reactions rather than hydrogenation reactions, which effectively convert heavy compounds into diesel-range fractions [36]. Zn/CRA deoxygenation produces hydrocarbons that predominantly fall in the C_{14}-C_{18} range and a high peak at C_{20}-C_{25} fraction [22].

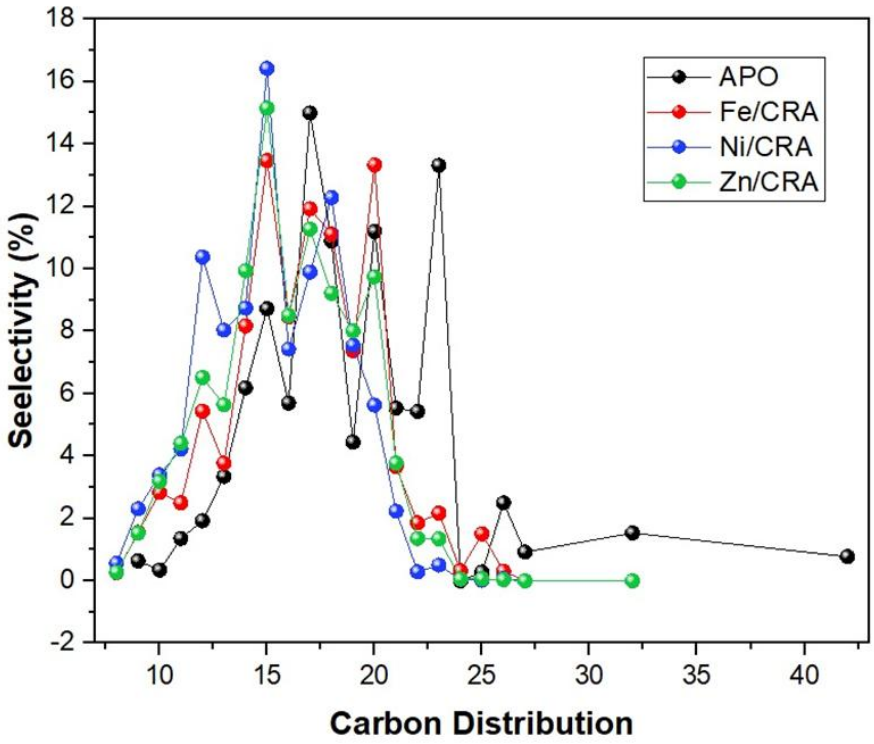

Figure 9 Carbon distribution of the APO deoxygenation using Fe/CRA, Ni/CRA, and Zn/CRA catalysts.

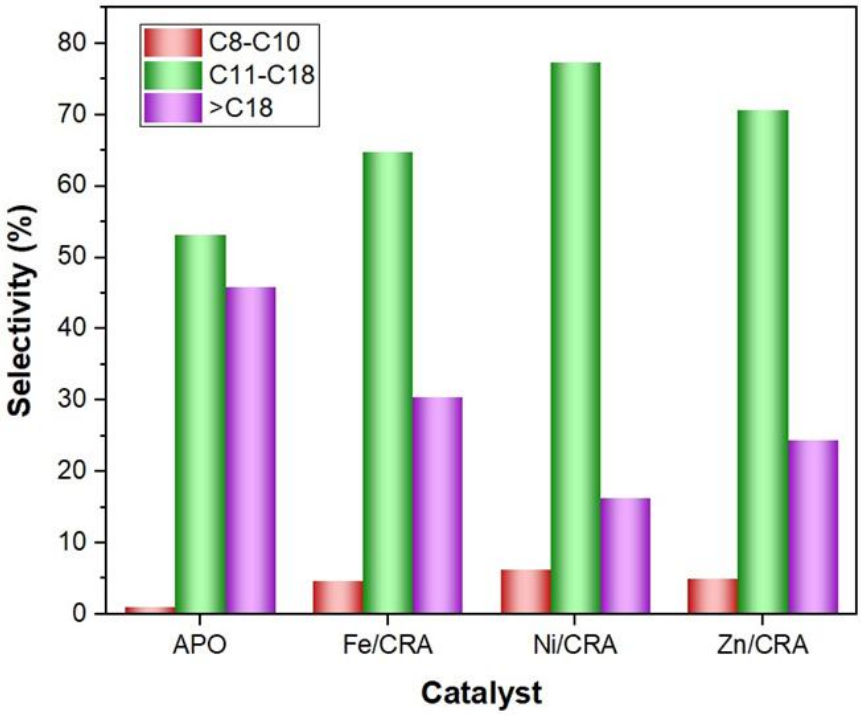

Figure 10 The distribution of hydrocarbon fractions by deoxygenation of APO using Fe/CRA, Ni/CRA, and Zn/CRA catalysts.

Figure 10 confirms the previous results regarding the distribution of hydrocarbons based on the range of carbon numbers. The initial APO oil has a high heavy fraction >C_{18} (45.91%). After the deoxygenation process, all CRA-metal-based catalysts convert the heavy fraction into the C_{11}-C_{18} fraction. Fe/CRA and Zn/CRA increase the C_{11}-C_{18} fraction to around 65% - 70%, indicating their ability to reduce heavy oil components, although some of the >C_{18} fraction is still present. Among the three catalysts, Ni/CRA shows the most optimal performance with the highest selectivity towards the diesel-range fraction (77.40%) while reducing the >C_{18} fraction to only 16.32%. In addition, Ni/CRA produced a slight increase in the C_8 - C_{10} fraction, which indicates the occurrence of partial cracking through the hydrodeoxygenation reaction [36].

Molecular composition of the APO and the deoxygenation product

Asphalt pyrolysis oil (APO) has a dark brown color that consists of hundreds of organic compounds and various oxygenates [42]. GC-MS analysis of the chemical components of APO before and after deoxygenation using Ni/CRA catalyst is shown in **Tables S1** - **S2**, respectively. Based on **Table S1** the initial APO consists of an oil fraction dominated by long hydrocarbon chains C > 18, such as pentacosane, hexacosane, 3-eicosene, 12-tricosanone, and nonacosane and long carbon chain ketones such as (2- and 9-heptadecanone, 3-octadecanone, 12-tricosanone), fatty acids (heptanoic acid, nonanoic acid, hexadecanoic acid), and unsaturated esters (octadec-9-enoic acid and methyl palmitate). The presence of these acids, ketones, and esters indicates that APO is acidic and less stable as a fuel. **Table S2** shows the chemical composition of APO after deoxygenation using Ni/CRA catalyst. The product was dominated by n-alkane and medium chain hydrocarbon fractions such as undecane, dodecane (and 2-methyl-dodecane), tridecane, pentadecane, hexadecane, heptadecane, and a small amount of heavy hydrocarbon fractions such as nonadecane, 1-eicosene, eicosane, docosane, and tricosane. While the oxygenate compound residues, such as carbonic acid decyl-tetradecyl ester, 10-undecenoic acid 2-methoxy methyl ester, Z-8-methyl-9-tetradecen-1-ol acetate, isolongifolol, and longifolenaldehyde are only in small amounts. This shows that the Ni/CRA catalyst can reduce oxygen content effectively through the

hydrogenation mechanism, while the thermal treatment cracking the heavy fraction into lighter hydrocarbon fractions [36].

Reaction mechanisms

Figure 11 shows the proposed reaction pathway for the catalytic deoxygenation of APO using CRA catalysts impregnated with Fe, Ni and Zn metals. The reaction pathway was established based on the product distribution and the composition of the liquid hydrocarbon formation provided by GC-MS analysis. Based on the reaction mechanism, the difference in selectivity to gas, coke, and liquid hydrocarbons for Fe/CRA and Ni/CRA catalysts stems from their fundamentally different hydrogenation capabilities and their dominant deoxygenation pathways. In Ni/CRA, oxygenated molecules are rapidly stabilized through efficient hydrogen activation at the Ni site, followed by hydrogenation of the C=C and C=O bonds. This rapid stabilization facilitates subsequent C-O bond cleavage via the hydrodeoxygenation pathway, producing stable liquid-range hydrocarbons and suppressing secondary reactions [14,20]. Consequently, gas and coke formation are significantly minimized [17-19]. In contrast, Fe/CRA shows limited hydrogen activation capability, resulting in insufficient stabilization of oxygenated intermediates, which subsequently undergo secondary cracking, condensation, and aromatization reactions, increasing gas and coke formation [43]. Therefore, inadequate hydrogenation in Fe/CRA shifts the reaction pathway toward gas and coke production, while effective hydrogenation in Ni/CRA directs the upgrading process toward selective liquid hydrocarbon formation and efficient removal of oxygenated compounds.

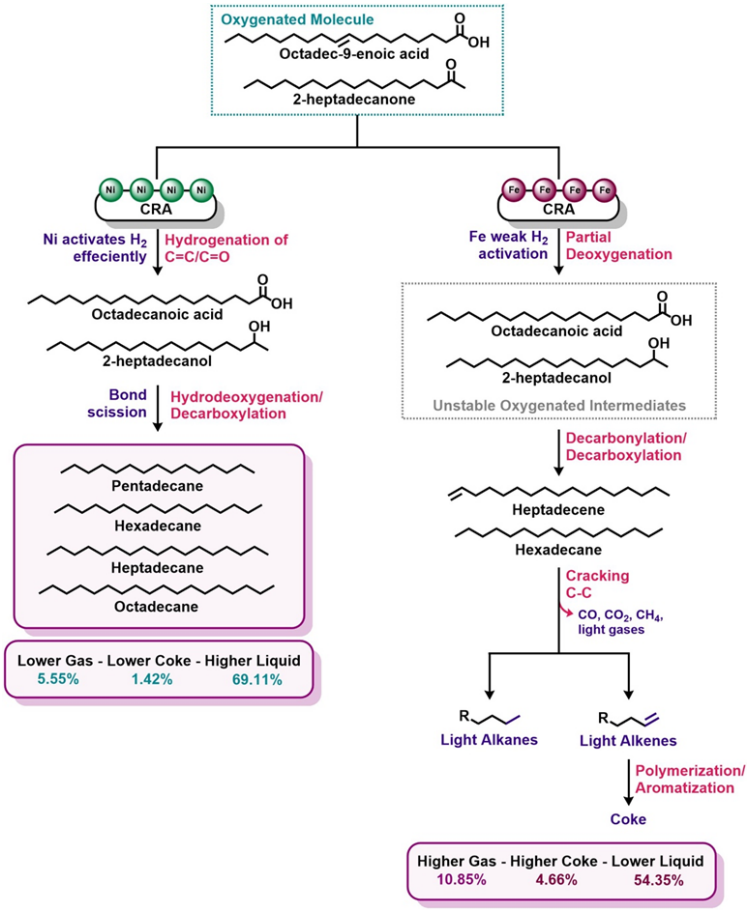

Figure 11 Reaction mechanism for the conversion of APO.

Table 4 presents a comprehensive catalytic activity of Ni/CRA against other similar catalysts, highlighting its superior performance. The waste Ni/marble catalyst was able to achieve very high conversion (95.2%), but its hydrocarbon yield was relatively low (55.9%), indicating the dominance of

excessive cracking and gas fraction formation [14]. Synthetic mesoporous-based catalysts such as 10%Ni/Al-MCM-41 and Ni-Cu/Al-MCM-41 produced moderate hydrocarbon yields (~53 - 61%) but required longer reaction times and higher temperatures, while Ni-carbon only achieved a hydrocarbon yield of around 60.1% even when operated at extreme temperatures (550 °C) [44,45]. $NiMo/Al_2O_3$ and $NiMoS_2/\gamma$-Al_2O_3 catalysts operating under hydrogen pressure showed lower hydrocarbon yields (≈50 -58%), reflecting limited hydrocarbon selectivity despite more complex reaction conditions [46,47]. In contrast, Ni/CRA was able to achieve 76.08% conversion and 65.03% hydrocarbon yield under relatively moderate reaction conditions (350 °C, 2 h, N_2 flow), indicating an optimal balance between activity and selectivity. The advantages of Ni/CRA come from the synergy between Ni active sites that effectively facilitate the cleavage of heavy C-O and C-C bonds, and the natural base matrix $CaCO_3$ in CRA that suppresses excessive cracking and coke formation. In addition, the use of CRA as a catalyst support provides promising advantages through the circular economy concept, making Ni/CRA an efficient, stable, and applicable catalyst for the upgrading of pyrolysis oil.

Table 4 Reported studies on catalytic cracking reaction on various catalysts.

Catalyst	Reaction condition	Conversion (%)	Hydrocarbons yield (%)	Ref
Ni/Marble waste	1 h 380 ºC N_2 Flow	95.2	55.92	[14]
10%Ni/Al-MCM-41	4h 350 °C N_2 Flow	68.53	~61.5	[44]
Ni-Cu/Al-MCM-41	1 h 400 ◦C N_2 Flow	-	53.1	[45]
15%Ni-Carbon	3 h 550 °C N_2 Flow	-	60.1	[10]
0.2-NiMoS2/γ-Al2O3	3 h 300 °C H_2 pressure	-	58.0	[46]
NiMo/Al2O3	1 h 350 °C H_2 pressure		50.83	[47]
Ni/CRA	2 h 350 °C N_2 Flow	76.08	65.03	This research

Conclusions

The CRA modified Ni, Fe, and Zn catalyst has successfully improved the quality of Asphalt Pyrolysis Oil (APO) products. GC-MS analysis showed that the initial APO was dominated by oxygenates and heavy fractions $>C_{18}$ (45.91%). After the deoxygenation reaction using Ni/CRA, the hydrocarbon fraction increases, the C_{11}-C_{18} fraction increases to 77.40%, and the $>C_{18}$ fraction decreases to 16.32%. The Ni/CRA catalyst also produces the highest liquid yield (69.11%) and the lowest coke (1.42%). The Ni-CRA catalyst promoted the hydrogenation and hydrogenolysis of oxygenate compounds (acids, ketones, esters), so it was effective in reducing oxygen content. Fe/CRA and Zn/CRA also showed an upgrading effect, although with lower activity than Ni/CRA. Overall, this study confirms that the use of CRA as a mineral-carbon-based catalyst not only provides a zero-waste approach to residual asphalt (CRA) but also produces an effective and economical catalyst for pyrolysis oil upgrading. The Ni/CRA catalyst proved to have the potential to produce higher-quality and low-oxygen pyrolysis oil, making it more suitable as a sustainable liquid fuel.

Acknowledgements

The authors would like to acknowledge Kementerian Pendidikan Kebudayaan Riset dan Teknologi, Jakarta 12920, Indonesia, under

Fundamental Grant (PDD) 1313/PKS/ITS/2025 for the financial and technical support.

Declaration of Generative AI in Scientific Writing

The authors acknowledge the use of a generative AI tool (ChatGPT by OpenAI) in the preparation of this manuscript, specifically for language editing and grammar correction. No content generation or data interpretation was performed using AI. The authors take full responsibility for the content and conclusions of this work.

CRediT author statement

Vicario Baroroh: Conceptualization, Methodology, Formal analysis, Investigation, Visualization, Writing – Original Draft. **Didik Prasetyoko:** Conceptualization, Methodology, Validation, Resources, Supervision, Writing – Review & Editing, Funding acquisition. **Stella Jovita:** Visualization, Formal analysis, Validation. **Jasmin Nur Anggia:** Investigation Visualization, Formal analysis, Validation. **Brigyta Savariell Kurniawan:** Investigation Visualization, Formal analysis, Validation. **Anggoro Dias Ainur Rasyid:** Editing, Formal analysis. **Hasliza Bahruji:** Formal analysis, Validation, Editing. **Khawiyatur Rivah:** Visualization, Formal analysis. **Ingelia Yuan Fernanda:** Visualization, Formal analysis. **Trias Alzatory Ersyada:** Visualization, Formal analysis. **Anjas Abimanyu:** Visualization, Formal analysis. **Nurul Asikin Mijan:** Visualization, Formal analysis. **Suprapto Suprapto:** Conceptualization, Methodology, Validation, Resources, Supervision, Writing – Review & Editing, Funding acquisition.

References

[1] J Hao, P Zong, Y Tian, J Zhang and Y Qiao. Distribution and chemical structure characteristic of the fast thermal-cracking products of Buton oil sand bitumen by Py-GC/TOF-MS and a fluidized bed reactor. *Energy Conversion and Management* 2019; **183**, 485-499.

[2] JL Sihombing, H Herlinawati, N Pulungan, L Simatupang, R Rahayu and AA Wibowo. Effective hydrodeoxygenation bio-oil via natural zeolite supported transition metal oxide catalyst. *Arabian Journal of Chemistry* 2023; **16(50)**, 104707.

[3] K Primerano, J Mirwald and B Hofko. Asphaltenes and maltenes in crude oil and bitumen: A comprehensive review of properties, separation methods, and insights into structure, reactivity and aging. *Fuel* 2024; **368**, 131616.

[4] Y Liu, Q Yao, M Sun and X Ma. Catalytic fast pyrolysis of coal tar asphaltene over zeolite catalysts to produce high-grade coal tar: An analytical Py-GC/MS study. *Journal of Analytical and Applied Pyrolysis* 2021; **156**, 105127.

[5] T He, Z Zhong and B Zhang. Bio-oil upgrading via ether extraction, looped-oxide catalytic deoxygenation, and mild electrocatalytic hydrogenation techniques. 2020; **34(8)**, 9725-9733.

[6] Z Guo, K Li, L Jiang, Y Ran, EK Sarkodie, J Yang, J Shi, S Liu, M Li, J Li, H Liu, Y Liang, H Yin and X Liu. Removal mechanisms of phosphate from water by calcium silicate hydrate supported on hydrochar derived from microwave-assisted hydrothermal treatment. *Environmental Technology & Innovation* 2022; **28**, 102942.

[7] P Zhang, M He, S Huo, F Li and K Li. Recent progress in metal-based composites toward adsorptive removal of phosphate: Mechanisms, behaviors, and prospects. *Chemical Engineering Journal* 2022; **446(2)**, 137081.

[8] R Tamim, D Prasetyoko, S Jovita, YL Ni'mah, RE Nugraha, H Holilah, H Bahruji, R Yusop, N Asikin-Mijan, AA Jalil, H Hartati and DD Anggoro. Low temperature pyrolysis of waste cooking oil using marble waste for bio-jet fuel production. *Renewable Energy* 2024; **232**, 121135.

[9] SF Basumatary, S Brahma, M Hoque, BK Das, M Selvaraj, S Brahma and S Basumatary. Advances in CaO-based catalysts for sustainable biodiesel synthesis. *Green Energy and Resources* 2023; **1(3)**, 100032.

[10] P Maneechakr and S Karnjanakom. Improving the Bio-oil quality via effective pyrolysis/deoxygenation of palm kernel cake over a metal (Cu, Ni, or Fe)-doped carbon catalyst. *ACS Omega* 2021; **6(30)**, 20006-20014.

[11] M Ambarita, D Ardiansyah, WW Schmahl, YM Pusparizkita, R Ismail, J Jamari and AP Bayuseno. Indirect mineral carbonation of natural asphalt extraction solid waste residue *via* pH and temperature control. *Case Studies in Chemical and Environmental Engineering* 2024; **9**, 100715.

[12] C Jia, H Yu, H Liu, H Qin and Q Wang. Pyrolysis characteristics of Indonesian oil sand in a fixed bed. *ACS Omega* 2022; **7(27)**, 23315-23321.

[13] N Widiarti, Wijianto, N Wijayati, Harjito, SBW Kusuma, D Prasetyoko and Suprapto. Catalytic activity of calcium oxide from fishbone waste in waste cooking oil transesterification process. *Jurnal Bahan Alam Terbarukan* 2017; **6(2)**, 97-106.

[14] R Tamim, D Prasetyoko, S Jovita, R Subagyo, YL Ni'Mah, H Holilah, H Bahruji, N Asikin-Mijan, AA Jalil, H Hartati and DD Anggoro. Ni-activated marble waste nanoparticles for catalyzed pyrolysis of waste cooking oil into hydrocarbon. *Renewable Energy* 2025; **248**, 123128.

[15] H Vicente, C Liu, AG Gayubo, P Cast and EA Pidko. Improving the dehydrogenation function and stability of Zn-modified ZSM-5 catalyst in methanol-to-aromatics reaction by Ca addition. *Applied Catalysis A: General* 2024; **683**, 119854.

[16] RSRM Hafriz, IN Sha, NA Ari, A Salmiaton, R Yunus, YH Tau and AH Shamsuddin. Effect of Ni/Malaysian dolomite catalyst synthesis technique on deoxygenation reaction activity of waste cooking oil. *Renewable Energy* 2021; **178**, 128-143.

[17] S Lv, J Yuan, X Peng, MB Cabrera, S Guo, X Luo and J Gao. Performance and optimization of bio-oil/Buton rock asphalt composite modified asphalt. *Construction and Building Materials* 2020; **264**, 120235.

[18] S Oh, HS Choi, IG Choi and JW Choi. Evaluation of hydrodeoxygenation reactivity of pyrolysis bio-oil with various Ni-based catalysts for improvement of fuel properties. *RSC Advances* 2017; **7(25)**, 15116-15126.

[19] X Yu and CT Williams. Recent applications of nickel and nickel-based bimetallic catalysts for hydrodeoxygenation of biomass-derived oxygenates to fuels. *Catalysis Science & Technology* 2023; **13(3)**, 802-825.

[20] A Gil and SA Korili. Progress and perspectives in the catalytic hydrotreatment of Bio-oils: Effect of the nature of the metal catalyst. *Industrial & Engineering Chemistry Research* 2024; **63(27)**, 11759-11775.

[21] LI Al-ali, O Elmutasim, KA Ali, N Singh and K Polychronopoulou. Transition Metal Phosphides (TMP) as a versatile class of catalysts for the hydrodeoxygenation reaction (HDO) of oil-derived compounds. *Nanomaterials* 2022; **12(9)**, 1435.

[22] Y Yee, S Thangalazhy-gopakumar, H Kiat, L Yee and S Gan. Effect of oxide catalysts on the properties of bio-oil from in-situ catalytic pyrolysis of palm empty fruit bunch fiber. *Journal of Environmental Management* 2019; **247**, 38-45.

[23] A Peter, B Chabot and E Loranger. Pre - and post - pyrolysis effects on iron impregnation of ultrasound pre - treated softwood biochar for potential catalysis applications. *SN Applied Sciences* 2021; **3**, 643.

[24] Y Wang, L Li, Z Liu and Z Ren. Frontier research and prospect of phosphate adsorption in wastewater by red mud: A review. *Desalination and Water Treatment* 2023; **310**, 86-108.

[25] RE Nugraha, H Purnomo, A Aziz, H Holilah, H Bahruji, N Asikin-Mijan, S Suprapto, YH Taufiq-Yap, AA Jalil, H Hartati and D Prasetyoko. The mechanism of oleic acid deoxygenation to green diesel hydrocarbon using porous aluminosilicate catalysts. *South African Journal of Chemical Engineering* 2024; **49**, 122-135.

[26] X Liu, F Shen and X Qi. Adsorption recovery of phosphate from aqueous solution by CaO-biochar composites prepared from eggshell and rice straw. *Science of The Total Environment* 2019; **666**, 694-702.

[27] NA Zul, S Ganesan, TS Hamidon, WD Oh and MH Hussin. A review on the utilization of calcium oxide as a base catalyst in biodiesel production. *Journal of Environmental Chemical Engineering* 2021; **9(4)**, 105741.

[28] M Kouser, B Chowhan, N Sharma and M Gupta. Transformation of waste toner powder into valuable Fe2O3 nanoparticles for the preparation of recyclable Co(II)-NH2-SiO2@Fe2O3 and its applications in the synthesis of

polyhydroquinoline and quinazoline derivatives. *ACS Omega* 2022; **7(51)**, 47619-47633.

[29] L Liu, S Fu, X Lv, L Yue, L Fan, H Yu, X Gao, W Zhu, W Zhang, X Li and W Zhu. A gas sensor with Fe2O3 nanospheres based on trimethylamine detection for the rapid assessment of spoilage degree in fish. *Frontiers in Bioengineering and Biotechnology* 2020; **8**, 567584.

[30] Z Mohammadpour and HR Zare. A comparative study on the effect of MWCNT as reinforcement on the corrosion parameters of different Ni–W/MWCNTs nanocomposite coatings in various corrosive media. *Metals and Materials International* 2018; **24**, 761-772.

[31] OS Vereshchagin, IA Chernyshova, MA Kuz and OV Frank-Kamenetskaya. Calcium carbonate precipitation behavior in the system Ca-Me2+-CO3-H2O (Me2+ = Co, Ni, Cu, Fe): Ion incorporation, effect of temperature and aging. *Minerals* 2023; **13(12)**, 1497.

[32] E Hadjittofis, SM Vargas, JD Litster and KLS Campbell. Exploring the role of crystal habit in the Ostwald rule of stages. *Proceedings Mathematical, Physical, and Engineering Sciences* 2022; **478(2258)**, 20210601.

[33] K Haiouani, S Hegazy, H Alsaeedi, M Bechelany and A Barhoum. Green synthesis of hexagonal-like ZnO nanoparticles modified with phytochemicals of clove (*Syzygium aromaticum*) and *Thymus capitatus* extracts: Enhanced antibacterial, antifungal, and antioxidant activities. *Materials* 2024; **17(17)**, 4340.

[34] S Dampang, E Purwanti, F Destyorini, SBKB Kurniawan, SRS Abdullah and MF Imron. Analysis of optimum temperature and calcination time in the production of CaO using seashells waste as CaCO3 source. *Journal of Ecological Engineering* 2021; **22(5)**, 221-228.

[35] J Qiao, Y Gao, K Zheng, C Shen, A Jia and Q Zhang. One-pot synthesis of magnetic core-shell Fe3O4@C nanospheres with Pt nanoparticle immobilization for catalytic hydrogenation of nitroarenes. *Applied Sciences* 2025; **15(10)**, 5773.

[36] Y Lv, H Wang, H Wu, Q Luo, L Wang and F Xiao. Silica modulation of raney nickel catalysts for selective hydrogenation. *Precision Chemistry* 2023; **1(5)**, 309-315.

[37] AN Hadi, MH Meteab and MK Mohammed. Influence of inclusion Sb2O3/NiO nanostructures on the morphological, microstructural, and optical characteristics of PVA polymeric for gamma-ray shielding applications. *Revue des Composites et des Matériaux Avancés* 2025; **35(3)**, 581-591.

[38] A Hamid, A Fadhel and S Azara. Studying the effect of irradiation time in preparing zinc oxide nanoparticles prepared by microwave method. *Digest Journal of Nanomaterials and Biostructures* 2022; **17(4)**, 1417-1422.

[39] Y Zhang, W Lu, D Han, H Guo, X Peng, W Zhu, N Xie, X Zuo, H Zhang, Q Pan and M Xie. Laboratory investigation of modified asphalt containing buton rock asphalt or ash from buton rock asphalt. *Case Studies in Construction Materials* 2023; **18**, 02124.

[40] N Nazarudin, YY Hans, O Alfernando, U Ulyarti and IB Adilina. Catalytic cracking of methyl ester derived from used cooking oil over Ni-impregnated activated charcoal catalyst. *Reaktor* 2022; **22(1)**, 21-27.

[41] C Mata, V Rojas-reinoso and JA Soriano. Experimental determination and modelling of fuel rate of injection: A review. *Fuel* 2023; **343**, 127895.

[42] S Collins, N Serge, K Regonne, Z Bilo and N Martin. Optimized biofuel production from *Triplochiton scleroxylon* sawdust via microwave-assisted pyrolysis and hydrocracking: Process analysis and production revenue forecasting with Aspen Plus. *Sustainable Chemistry for the Environment* 2025; **12**, 100294.

[43] MA Nawaz, R Blay-roger, M Saif, F Meng, LF Bobadilla. TR Reina and JA Odriozola. Redefining the symphony of light aromatic synthesis beyond fossil fuels: A journey navigating through a Fe-Based/HZSM-5 tandem route for syngas conversion. *ACS Catalysis* 2024; **14(20)**, 15150-15196.

[44] RE Nugraha, D Prasetyoko, H Bahruji, S Suprapto, N Asikin-Mijan, TP Oetami, AA Jalil, DVN Vo and YH Taufiq-Yap. Lewis acid Ni/Al-MCM-41 catalysts for H2-free deoxygenation of *Reutealis trispermaoil* to biofuels. *RSC Advances* 2021; **11(36)**, 21885-21896.

[45] LGG Pereira, Q Yuan, HJ Heeres, SB Lima and CAM Pires. Catalytic hydrotreatment of fast pyrolysis oils using Ni-Cu / Al-MCM-41 catalysts. *Journal of Analytical and Applied Pyrolysis* 2024; **181**, 106593.

[46] D Prangklang, D Tumnantong, B Yoosuk, C Ngamcharussrivichai and P Prasassarakich. Selective deoxygenation of waste cooking oil to diesel-like hydrocarbons using supported and unsupported NiMoS2 catalysts. *ACS Omega* 2023; **8(43)**, 40921-40933.

[47] C Muangsuwan, W Kriprasertkul, S Ratchahat, C Liu, P Posoknistakul, N Laosiripojana and C Sakdaronnarong. Upgrading of light bio-oil from solvothermolysis liquefaction of an oil palm empty fruit bunch in glycerol by catalytic hydrodeoxygenation using NiMo/Al2O3 or CoMo/Al2O3 catalysts. *ACS Omega* 2021; **6(4)**, 2999-3016.